A&A 370, 754–764 (2001)
DOI: 10.1051/0004-6361:20010322

Astronomy & Astrophysics

Lensing Sunyaev-Zel'dovich clusters

M. Bartelmann⋆

Max-Planck-Institut für Astrophysik, PO Box 1317, 85741 Garching, Germany

Received 29 September 2000 / Accepted 22 February 2001

Abstract. Full-sky microwave surveys like the upcoming *Planck* satellite mission will detect of order 10^4 galaxy clusters through their thermal Sunyaev-Zel'dovich effect. I investigate the properties of the gravitationally lensing subsample of these clusters. The main results are: (1) The combined sample comprises $\gtrsim$70% of the complete sample. (2) It is confined to redshifts 0.2 ± 0.1, and to masses $(5 \pm 3)\ 10^{14}\,M_\odot$. (3) Using a particular measure for the weak lensing effect, viz. the aperture mass, cluster masses can be determined with a relative accuracy of ∼20% if their density profile is known. Consequently, the mass function of the combined sample can accurately be measured. (4) For low-density universes, I predict a sharp peak in the measured (aperture) mass function near $5\ 10^{14}\,M_\odot$ and explain its origin, showing that the peak will be absent in high-density universes. (5) The location of the peak and the exponential decrease of the mass function on its high-mass side will allow the determination of the amplitude of the dark-matter power spectrum on the cluster scale and the baryon fraction in clusters, and constrain the thermal history of the intracluster gas.

Key words. galaxies: clusters: general – cosmic microwave background – gravitational lensing

1. Introduction

Upcoming full-sky surveys in the microwave regime, like the *Planck* mission (Bersanelli et al. 1996), with angular resolutions of order $(5-10)'$ and sensitivities of micro-Kelvins, will detect thousands of galaxy clusters through their thermal Sunyaev-Zel'dovich effect. This effect arises because hot thermal electrons in the intracluster plasma Compton-upscatter the much colder microwave-background photons, re-distributing them from the low-frequency part of the spectrum below 218 GHz to the high-frequency part (Sunyaev & Zel'dovich 1972, 1980; Rephaeli 1995; Birkinshaw 1999).

At angular resolutions of a few arc minutes, most clusters will be barely resolved or unresolved (e.g. Aghanim et al. 1997; Hobson et al. 1998). Detailed cluster studies with the CMB survey data alone will therefore not be possible. In combination with optical, radio, or X-ray follow-up observations, however, the rich cluster samples detected in the microwave regime can be used to extract a wealth of cosmological information.

Promising additional information can be gained exploiting the gravitational lensing effects of the Sunyaev-Zel'dovich cluster sample. While strong lensing effects depend on the accurate alignment of randomly distributed background sources with respect to the cluster lenses, weak lensing is much less affected by stochastic effects. The question therefore arises what kind of information can be extracted from weak-lensing follow-up observations of the cluster sample produced by CMB missions such as *Planck*.

In this paper, I discuss in Sect. 2 the detection of clusters by *Planck* and the properties of the resulting cluster sample. In Sect. 3, weak gravitational lensing is introduced and applied to the cluster sample. The mass distribution of the combined sample is discussed in Sect. 4, and it is shown how it can be measured. The main results are summarised and discussed in Sect. 5.

2. Planck's cluster sample

2.1. Assumptions

We assume that the cluster population follows scaling relations derived from the spherical collapse model. The virial radius r_{200} is defined such that the mean overdensity of the halo within r_{200} is 200 times the critical density. This implies the relation

$$r_{200} = \left(\frac{GM}{100\,H^2(z)}\right)^{1/3} \tag{1}$$

between r_{200} and halo mass M. The Hubble function at redshift z is $H(z)$. Temperature T and virial mass M are assumed to be related by

$$kT = (kT)_{15}\,M_{15}^{2/3}\,(1+z)\left(\frac{\Omega_0}{\Omega(z)}\right)^{1/3}\left(\frac{\Delta_\mathrm{c}}{178}\right)^{1/3} \tag{2}$$

(e.g. Eke et al. 1996; Navarro et al. 1995), where $M_{15} = M/10^{15}\,M_\odot$ and $(kT)_{15} = 6.03\,\mathrm{keV}$ is the temperature of

⋆ e-mail: mbartelmann@mpa-garching.mpg.de

a cluster with $M_{15} = 1$ (Mathiesen & Evrard 2001). The density parameter at redshift z is $\Omega(z)$, and Δ_c is the mean overdensity of a virialised sphere,

$$\Delta_\mathrm{c} = 9\pi^2 \left[1 + \alpha\,(\Omega - 1) + \Omega^\beta\right] \tag{3}$$

with

$$(\alpha, \beta) = \left\{ \begin{array}{l} (0.1210, 0.6756) \ \text{open} \\ (0.7076, 0.4403) \ \text{flat} \end{array} \right\} \ \text{cosmology} \tag{4}$$

(Stoehr 1999).

Moreover, we assume that the total number N of thermal electrons within a cluster's virial radius is proportional to the virial mass,

$$N_\mathrm{e} = \frac{1 + f_\mathrm{H}}{2}\, f_\mathrm{B}\, \frac{M}{m_\mathrm{p}}, \tag{5}$$

where f_B is the baryon fraction of the cluster mass, f_H is the hydrogen fraction of the baryonic mass, $f_\mathrm{H} \approx 0.76$, and m_p is the proton mass. From X-ray data of an ensemble of 45 clusters, Mohr et al. (1999) derived $f_\mathrm{B} = 0.075\,h^{-3/2}$. Myers et al. (1997) used thermal Sunyaev-Zel'dovich observations in three nearby Abell clusters to find a lower baryonic mass fraction of $f_\mathrm{B} = 0.061\,h^{-1}$, but this interpretation strongly depends on cluster shape (cf. Grego et al. 2000). We adopt the baryon fraction by Mohr et al. below.

We describe the projected thermal electron density with a King profile, i.e. a β model with $\beta = 1$,

$$n_\mathrm{e,2D}(\theta) = n_0 \left[1 + \left(\frac{\theta}{\theta_\mathrm{c}}\right)^2\right]^{-1}, \tag{6}$$

where θ_c is the angular core radius. For our choice of $\beta = 1$, the entropy-driven cluster evolution model (Bower 1997) predicts

$$r_\mathrm{c} = r_\mathrm{c0}\,(1 + z)^{-1/2(1+\epsilon)}, \tag{7}$$

where ϵ is the entropy parameter. We put $\epsilon = 0$ here corresponding to the constant-entropy model (Kaiser 1991; Evrard & Henry 1991), resulting in a much more gentle redshift evolution of the core radius than predicted by the self-similar evolution model (Kaiser 1986). However, for poorly resolved cluster observations like those expected from *Planck*, the choice of ϵ only marginally affects the results. We further choose $r_\mathrm{c0} = 0.13\,\mathrm{Mpc}/h$.

Conventionally, the number density of dark-matter haloes is described by the Press-Schechter model (Press & Schechter 1974). The Press-Schechter mass function can be written as

$$n_\mathrm{PS}(M, z) = \frac{\bar\rho}{\sqrt{2\pi}\, D_+(z)\, M^2} \left(1 + \frac{n}{3}\right) \left(\frac{M}{M_*}\right)^{(n+3)/6} \times \exp\left[-\frac{1}{2\,D_+^2(z)} \left(\frac{M}{M_*}\right)^{(n+3)/3}\right], \tag{8}$$

where M_* and $\bar\rho$ are the nonlinear mass today and the mean background density *at the present epoch*, and $D_+(z)$ is the linear growth factor of density perturbations, normalised to unity today, $D_+(0) = 1$. Finally, n is the effective exponent of the dark-matter power spectrum at the cluster scale, $n \approx -1$.

Sheth & Tormen (1999) recently modified the mass function (8), and Sheth et al. (1999) introduced ellipsoidal rather than spherical collapse. Jenkins et al. (2001) derived the mass function of dark-matter haloes from numerical simulations and found a fitting formula very close to Sheth & Tormen's, but with lower amplitude at the high-mass end. We used all three mass functions here and found that deviations from the Press-Schechter prediction noticeably change the results, so we used the fitting formula by Jenkins et al. for the results shown.

2.2. Cluster detection

The Sunyaev-Zel'dovich effect is determined by the Compton-y parameter,

$$y(\boldsymbol{\theta}) = \frac{kT}{m_\mathrm{e}c^2}\sigma_\mathrm{T} \int \mathrm{d}l\, n_\mathrm{e}(\boldsymbol{\theta}, l), \tag{9}$$

if the gas distribution in the cluster is isothermal. The thermal, three-dimensional electron density is written as $n_\mathrm{e}(\boldsymbol{\theta}, l)$ to indicate that it depends on the direction $\boldsymbol{\theta}$ on the sky, and σ_T is the Thomson scattering cross section.

In the absence of background noise, the total Compton-y parameter seen from a galaxy cluster would be

$$Y = \int \mathrm{d}^2\boldsymbol{\theta}\, y(\boldsymbol{\theta}) = \frac{kT}{m_\mathrm{e}c^2}\, \frac{\sigma_\mathrm{T}}{D_\mathrm{d}^2}\, N_\mathrm{e}, \tag{10}$$

where D_d is the angular-diameter distance to the cluster and N_e is the total number of (thermal) electrons in the cluster; see Eq. (5). Since y is dimension-less, Y is effectively a solid angle.

The angular resolution of *Planck* will not allow to spatially resolve low-mass clusters, and even high-mass clusters will be barely resolved (Aghanim et al. 1997; Hobson et al. 1998). There will therefore be a Compton-y background y_bg dominated by low-mass clusters, since their much higher number density over-compensates their lower individual contributions. An ideally isotropic background would not matter since it could be completely removed. It is therefore the average background fluctuation level, Δy_bg, that we have to take into account. Moreover, *Planck* will see the clusters convolved with its beam profile $b(\boldsymbol{\theta})$.

We therefore adopt the following cluster detection criterion for *Planck* (see also Bartlett 2000). Let the beam-convolved Compton-y profile of a cluster be

$$\bar y(\boldsymbol{\theta}) = \int \mathrm{d}^2\theta'\, y(\boldsymbol{\theta}')\, b(\boldsymbol{\theta} - \boldsymbol{\theta}'). \tag{11}$$

A cluster is assumed to be detectable by *Planck* if its integrated, beam-convolved Compton-y parameter is sufficiently large, i.e.

$$\bar Y = \int \mathrm{d}^2\theta\, \bar y(\boldsymbol{\theta}) \geq \bar Y_\mathrm{min}, \tag{12}$$

where the integral covers the area where the integrand sufficiently exceeds the background fluctuations, $\bar{y} \geq \nu\Delta y_{\rm bg}$. We choose $\nu = 3$ in the following, so that the integration covers an area in which the integrand is at least 3σ above the rms background (cf. Eq. (18) below).

In evaluating (12), we use assumption (6) that the thermal electron density follows a King profile. Then,

$$y(\boldsymbol{\theta}) = y_0 \left[1 + \left(\frac{\theta}{\theta_{\rm c}}\right)^2\right]^{-1}, \tag{13}$$

with the angular core radius $\theta_{\rm c}$. Approximating the beam profile with a Gaussian,

$$b(\boldsymbol{\theta}) = \frac{1}{2\pi\sigma_{\rm B}} \exp\left(-\frac{\boldsymbol{\theta}^2}{2\sigma_{\rm B}^2}\right), \tag{14}$$

the beam-convolved Compton-y profile is,

$$\bar{y}(\boldsymbol{\theta}) = 2a{\rm e}^{-ax^2} \int_0^\infty x'{\rm d}x' \, \frac{\exp(-ax'^2)}{1+x'^2} {\rm I}_0(2axx'), \tag{15}$$

where $a \equiv \theta_{\rm c}^2/2\sigma_{\rm B}^2$, $x \equiv \theta/\theta_{\rm c}$, and ${\rm I}_0(x)$ is the zeroth-order modified Bessel function of the first kind. For wide beams, as in the case of *Planck*, the integral (15) can be well approximated by

$$\begin{aligned}\bar{y}(\theta) \;\approx\; & \frac{a{\rm e}^{-ax^2}}{4} \left[ax^2(4+ax^2(1-a))\right. \\ & \left. + {\rm e}^a(a^2x^2-2)^2 E_1(a)\right], \end{aligned} \tag{16}$$

where $E_1(a)$ is the first-order exponential integral. This expression has the advantage of being much more easily evaluated numerically than the integral (15). Ignoring the background fluctuations, $\bar{Y}$ from (12) equals Y from (10), as it should.

Finally, the background level is given by

$$\begin{aligned} y_{\rm bg} \;&=\; \int {\rm d}z \left|\frac{{\rm d}V}{{\rm d}z}\right| (1+z)^3 \int {\rm d}M \, n_{\rm PS}(M,z) \, Y(M,z) \\ &=\; \int {\rm d}M \int {\rm d}V \, Y(M,z) \, \frac{{\rm d}^2N(M,z)}{{\rm d}M{\rm d}V}, \end{aligned} \tag{17}$$

where ${\rm d}V$ is the cosmic volume per unit redshift and unit solid angle, $n_{\rm PS}(M,z)$ is the cluster mass function (8), and $Y(M,z)$ is the integrated Compton-y parameter from (10) expressed in terms of cluster mass M and redshift z (e.g. Barbosa et al. 1996; Da Silva et al. 1999). Neglecting cluster correlations, background fluctuations are due to Poisson fluctuations in the number of clusters per unit mass and volume. The rms background fluctuation is then

$$\Delta y_{\rm bg} = \left[\int {\rm d}M \int {\rm d}V \, Y^2(M,z) \, \frac{{\rm d}^2N(M,z)}{{\rm d}M{\rm d}V}\right]^{1/2}. \tag{18}$$

Taking cluster correlations into account would slightly increase $\Delta y_{\rm bg}$ above the fluctuation (18). However, since the volume integral extends along the line-of-sight over length scales much larger than the cluster correlation scale, it is justified to assume a Poissonian cluster distribution, even if the beam size should become comparable to the cluster correlation scale.

Although only undetected clusters contribute to the background and its fluctuation, the mass integral can be extended to infinity because of the steep decline of the mass function. While $y_{\rm bg}$ is a few times 10^{-6} depending on cosmology (e.g. Barbosa et al. 1996; da Silva et al. 2000), the background fluctuation $\Delta y_{\rm bg}$ increases from 5 10^{-8} for ΛCDM to 1.3 10^{-7} for $\Omega_0 = 1$.

The sensitivity limit $Y_{\rm min}$ can be derived from the nominal (antenna) temperature sensitivity of *Planck*, i.e. $\Delta T/T \geq 2\ 10^{-6}$ (Puget et al. 1998). The beam-integrated Sunyaev-Zel'dovich effect changes the flux by $\Delta F_\nu = 2\,Y\,I_\nu$. This leads to a change $\Delta I_\nu = \Delta F_\nu/\delta\Omega$ in specific intensity across a beam of solid angle $\delta\Omega$. The two expressions imply

$$Y \geq \frac{\Delta I_\nu}{I_\nu} \frac{\delta\Omega}{2} = \frac{\Delta T}{T} \frac{\delta\Omega}{2}. \tag{19}$$

With $\delta\Omega \approx 50$ arcmin^2 for the relevant *Planck* beams, expression (19) implies $Y_{\rm min} \approx 10^{-4}\,$arcmin^2 (see also Haehnelt 1997). Unless mentioned otherwise, we will assume $Y_{\rm min} = 3\ 10^{-4}\,$arcmin^2 below for a conservative limit.

Figure 1 shows contours of the number density in the M-z plane of clusters detectable by *Planck*. A low-density, flat CDM universe with $\Omega_0 = 0.3$, $\Omega_\Lambda = 0.7$ and $h = 0.7$ was adopted and normalised to match the local abundance of massive clusters (White et al. 1993; Eke et al. 1996; Viana & Liddle 1996). Following the results by Mohr et al. (1999), the baryon fraction is set to $f_{\rm B} = 13\%$. Choosing a higher or lower baryon fraction would shift the sharp upper edge of the contours in Fig. 1 to slightly higher or lower redshifts, respectively. The contours start at $10^{-10.5}\ M_\odot^{-1}$ and are separated by 0.2 dex. While the solid contours were obtained using the detection criteria discussed above, the dotted contours ignore the effects of beam convolution and background contamination. The axes are plotted logarithmically to emphasise the effect of the detailed detection criteria.

While spatially resolved observations of the thermal Sunyaev-Zel'dovich effect in clusters are independent of the cluster redshift, unresolved observations like those by *Planck* do depend on redshift through the distance factor in Eq. (10). The physical size of a given beam grows with distance, hence a cluster of given physical size shrinks with distance compared to the beam, and the background contamination grows. Therefore, taking beam convolution and background into account, the high-redshift part of the low-mass Sunyaev-Zel'dovich cluster population is removed. The background fluctuations impede in several ways on the possibility to discriminate cosmologies through the number of Sunyaev-Zel'dovich clusters detectable for *Planck*, as da Silva et al. (2000) suspected earlier. On the one hand, reducing Ω_0 leads to slower evolution of the cluster number density (Richstone et al. 1992) and larger cosmic volume per unit redshift, but a substantial part of these clusters is not visible to *Planck*

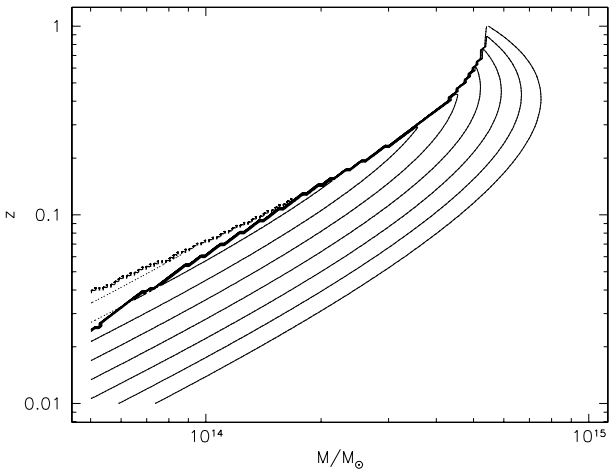

Fig. 1. Contours of the number density in the M-z plane of clusters which will be detectable for *Planck*. The lowest contour level is at $10^{-10.5}\,M_\odot^{-1}$, and the levels are logarithmically spaced at 0.2 dex. Dotted contours ignore the effects of beam convolution and background fluctuations. Note the logarithmic axes

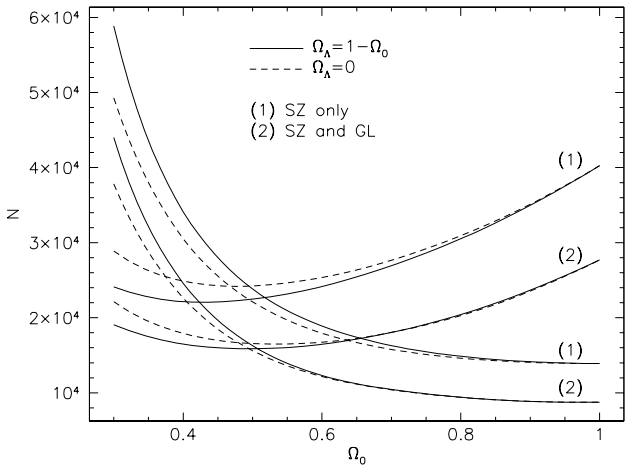

Fig. 2. The number of detectable Sunyaev-Zel'dovich clusters is plotted against Ω_0, assuming $\Omega_\Lambda = 0$ or $\Omega_\Lambda = 1 - \Omega_0$. Four pairs of curves are plotted. The solid curve of each pair was calculated for a flat, the dashed curve for an open model with given Ω_0. The almost horizontal curves assume $f_\mathrm{B} = 0.13$. For the monotonically falling set of curves, f_B varies according to the primordial nucleosynthesis constraint. The upper curves ignore lensing, the lower curves take it into account, as indicated

because of the dependence of the integrated y parameter on distance. The background increases with cluster number, so the relative background fluctuations decrease. The net effect is a very minor change of the detectable cluster number with cosmology, as shown in Fig. 2.

The figure shows four pairs of curves. One curve per pair represents a flat universe, the other an open universe, as indicated. The almost horizontal curves were calculated for a constant baryon fraction, $f_\mathrm{B} = 0.13$, while the baryon fraction varies according to the constraint from primordial nucleosynthesis, $f_\mathrm{B} = \Omega_\mathrm{B}/\Omega_0 = 0.024/\Omega_0\,h^2$ (e.g. Schramm 1998 for a review). The upper curves show the number of Sunyaev-Zel'dovich clusters detectable for *Planck*. The lower curves take gravitational lensing into account, as detailed in Sect. 3 below. For constant baryon fraction, the cluster number changes with Ω_0 by at most a factor of two, and it drops by a factor of $\sim$3 if the baryon fraction is fixed by primordial nucleosynthesis. The gravitationally lensing subsample comprises more than 70% of the full sample, quite independent of cosmology.

3. Lensing effects of the cluster sample

We give only a very brief summary of weak lensing by clusters here. For a detailed review, see Bartelmann & Schneider (2001).

3.1. Relevant properties of the aperture mass

Schneider (1996) suggested quantifying the weak-lensing effects of dark-matter haloes with the *aperture mass*,

$$M_\mathrm{ap}(\theta) = \int \mathrm{d}^2\boldsymbol{\vartheta}\,\kappa(\boldsymbol{\vartheta})\,U(|\boldsymbol{\vartheta}|), \tag{20}$$

which is an integral over the lensing convergence κ within a circular aperture with (angular) radius θ, weighted by a function $U(\vartheta)$ which vanishes outside the aperture. The prime advantage of M_ap is that it can directly be determined from the measured tidal distortions of background-galaxy images in the chosen aperture, provided $U(\vartheta)$ is compensated, i.e.

$$\int_0^\theta \mathrm{d}^2\vartheta\,\vartheta U(\vartheta) = 0. \tag{21}$$

A broad class of weight functions satisfies this condition. We will follow Schneider's suggestion and take

$$U(\vartheta) = \frac{9}{\pi\theta^2}\left[1-\left(\frac{\vartheta}{\theta}\right)^2\right]\left[\frac{1}{3}-\left(\frac{\vartheta}{\theta}\right)^2\right] \tag{22}$$

within the aperture, and $U(\vartheta) = 0$ outside.

Schneider (1996) also calculated the dispersion of M_ap due to the finite number of randomly distributed background galaxies and their intrinsic ellipticities. Assuming typical values for the number density n_g of suitably bright background galaxies and for the dispersion σ_ϵ of their intrinsic ellipticities, he found

$$\sigma_\mathrm{M}(\theta) = 0.016\left(\frac{n_\mathrm{g}}{30\,\mathrm{arcmin}^2}\right)^{-1/2}\left(\frac{\sigma_\epsilon}{0.2}\right) \times\left(\frac{\theta}{1\,\mathrm{arcmin}}\right)^{-1}. \tag{23}$$

For a singular isothermal sphere with Einstein radius θ_E, $\kappa(\vartheta) = \theta_\mathrm{E}/2\vartheta$, and

$$M_\mathrm{ap}^\mathrm{(SIS)}(\theta) = \frac{4}{5}\frac{\theta_\mathrm{E}}{\theta}. \tag{24}$$

The Einstein radius is proportional to the squared velocity dispersion σ_v^2 of the singular isothermal sphere, $\theta_\mathrm{E} \propto \sigma_v^2$.

Since the virial mass scales with velocity dispersion as $M \propto \sigma_v^3$, the aperture mass essentially measures $M^{2/3}$ when applied to a singular isothermal sphere. According to (23), the signal-to-noise ratio of $M_{\rm ap}$ for a singular isothermal sphere is independent of the aperture size θ, since both $M_{\rm ap}$ and $\sigma_{\rm M}$ scale as θ^{-1} in this case.

The situation is somewhat more complicated for the density profile suggested by Navarro et al. (1997),

$$\rho(r) = \frac{\rho_{\rm crit}\,\delta_{\rm c}}{(r/r_{\rm s})(1+r/r_{\rm s})^2}, \tag{25}$$

where $\rho_{\rm crit}$ is the critical density and $\delta_{\rm c}$ is a characteristic overdensity. The characteristic radial scale $r_{\rm s}$ is related to the virial radius through $r_{\rm s} = r_{200}/c$, where c is the concentration parameter. Bartelmann (1996) showed that the NFW profile has the lensing convergence

$$\kappa(x) = \frac{2\kappa_{\rm s}}{1-x^2}\left(1 - \frac{2}{\sqrt{1-x^2}}\mathrm{arctanh}\sqrt{\frac{1-x}{1+x}}\right), \tag{26}$$

with the convergence scale

$$\kappa_{\rm s} \equiv \frac{\rho_{\rm crit}\delta_{\rm c} r_{\rm s}}{\Sigma_{\rm cr}}, \tag{27}$$

where

$$\Sigma_{\rm cr} = \frac{c^2}{4\pi G}\left(\frac{D_{\rm s}}{D_{\rm d}D_{\rm ds}}\right) \tag{28}$$

is the critical surface mass density of a gravitational lens. The angular diameter distances to the lens, the source, and from the lens to the source are $D_{\rm d,s,ds}$, respectively.

Navarro et al. (1997) described how the parameters $\delta_{\rm c}$ and $r_{\rm s}$ are related to the virial mass M of the halo. Hence, despite the two formal parameters in the profile (25), it is entirely determined once the halo mass is fixed. The statistics of dark-matter haloes described bt the NFW density profile has also been investigated by Kruse & Schneider (1999).

Unfortunately, there is no closed expression for the aperture mass of an NFW profile. Progress can be made, however, under the assumption that the aperture radius θ is smaller than the angular scale radius, $\theta < \theta_{\rm s} = r_{\rm s}/D_{\rm d}$. With

$$t \equiv \frac{\theta}{\theta_{\rm s}}, \tag{29}$$

one can show by means of Taylor expansions that

$$M_{\rm ap}^{\rm (NFW)}(t) \approx \kappa_{\rm s}\left[1 + t^2\left(\frac{19}{32} + \frac{3}{4}\ln\frac{t}{2}\right) + t^4\left(\frac{77}{160} + \frac{3}{4}\ln\frac{t}{2}\right)\right]. \tag{30}$$

In other words, $M_{\rm ap}^{\rm (NFW)} \to \kappa_{\rm s}$ in the limit of small apertures. Within the mass range of galaxy clusters, $\rho_{\rm crit}\delta_{\rm c}$ is essentially a constant. Given the geometry of the lens system, $M_{\rm ap}^{\rm (NFW)}$ therefore essentially measures the scale radius $r_{\rm s}$ or, equivalently, $M^{1/3}$.

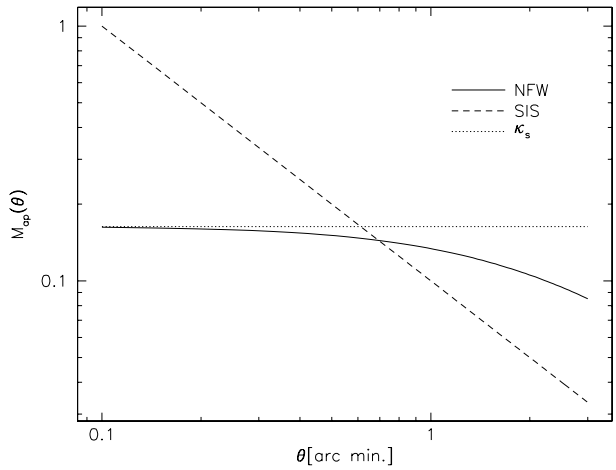

Fig. 3. The aperture mass $M_{\rm ap}(\theta)$ is plotted against aperture radius θ for an NFW halo of mass 5 $10^{14}\,M_\odot$ at redshift 0.2 lensing sources at redshift 1.5. The dotted curve shows $\kappa_{\rm s}$, the dashed curve illustrates the $1/\theta$ behaviour of $M_{\rm ap}(\theta)$ for a singular isothermal sphere. As explained in the text, $M_{\rm ap} \to \kappa_{\rm s}$ for $\theta \to 0$, and $M_{\rm ap}$ depends much more weakly on aperture size for an NFW halo than for a SIS

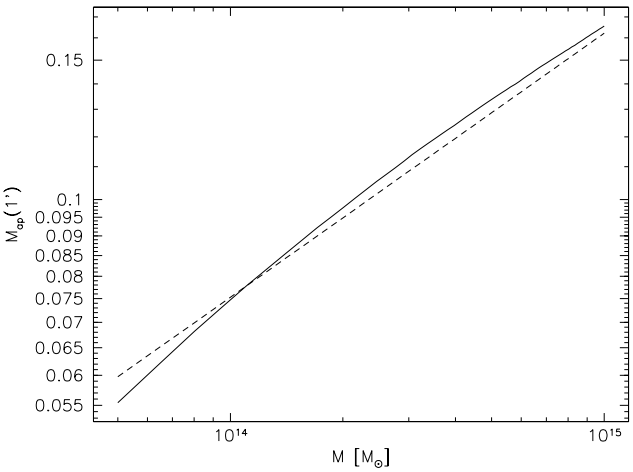

Fig. 4. The aperture mass $M_{\rm ap}(\theta)$ with $\theta = 1'$ is plotted against virial mass for haloes at redshift 0.2 lensing sources at redshift 1.5. The dashed curve shows the $M_{\rm ap} \propto M^{1/3}$ behaviour expected for sufficiently massive haloes

We thus see two important differences between the aperture masses of singular isothermal spheres and NFW profiles: For the latter, the aperture mass depends much more weakly on the halo mass and on the aperture size than for the former. Among other things, this implies with Eq. (23) that the signal-to-noise ratio for the aperture mass of an NFW halo decreases with decreasing aperture size. Figures 3 and 4 illustrate these results.

3.2. Dependence on source redshifts

Clearly, $M_{\rm ap}$ depends on the redshift of the background sources used to measure the gravitational shear.

In presence of a (normalised) source redshift distribution $p(z_\mathrm{s})$, the aperture mass of a halo at redshift z becomes

$$\bar{M}_\mathrm{ap}(\theta;z) = \int_z^\infty \mathrm{d}z_\mathrm{s}\, M_\mathrm{ap}(\theta;z,z_\mathrm{s})\, p(z_\mathrm{s}). \tag{31}$$

A useful and sufficiently accurate representation of the source redshift distribution is

$$p(z_\mathrm{s}) = \frac{\beta}{z_0^3\Gamma(3/\beta)}\, z^2\, \exp\left[-\left(\frac{z}{z_0}\right)^\beta\right], \tag{32}$$

for which we choose $z_0 = 1.0$ and $\beta = 1.5$ (Smail et al. 1995). Since M_ap is linear in κ, (31) amounts to replacing κ_s in (26) by its source-redshift averaged counterpart. Unless stated otherwise, the source redshift average (31) will from now on implicitly be applied.

3.3. Lensing Sunyaev-Zel'dovich clusters

We can now ask: What fraction of the cluster sample detectable for *Planck* will produce significant lensing effects? The significance of weak lensing by any given cluster of mass M and redshift z can be estimated by means of the signal-to-noise ratio $\mathcal{S}(\theta) = M_\mathrm{ap}(\theta)/\sigma_\mathrm{M}(\theta)$, where $\sigma_\mathrm{M}(\theta)$ is the dispersion (23). Then, the condition $\mathcal{S} \geq \mathcal{S}_\mathrm{min}$ defines a region in the M-z plane within which clusters produce a significant weak-lensing effect. We note that the numerical evaluation of that condition needs to take into account that the dispersion $\sigma_\mathrm{M}(\theta)$ depends on cluster redshift because the number density of sources, n_g, does: Only sources at redshifts higher than the cluster contribute to the measured tidal field.

The sample of clusters which can be detected by *Planck and* optically through their lensing effect is then determined by the two conditions

$$Y \geq Y_\mathrm{min} \quad \text{and} \quad \mathcal{S} \geq \mathcal{S}_\mathrm{min}. \tag{33}$$

We will assume $\mathcal{S}_\mathrm{min} = 5$ in the following, corresponding to highly significant detections of the weak-lensing signal.

Figure 5 shows contours of the number density in the M-z plane of Sunyaev-Zel'dovich clusters that are efficient weak lenses. Although the sample appears to be substantially reduced, Fig. 2 shows that this is not the case: The efficiently lensing Sunyaev-Zel'dovich cluster sample still comprises more than 70% of the original Sunyaev-Zel'dovich sample. In other words, the majority of clusters that *Planck* will detect as Sunyaev-Zel'dovich sources will also be detectable in the optical as efficient gravitational lenses. On the whole sky, a few times 10^4 such clusters are expected, quite independent of cosmological parameters (see Fig. 2; cf. Barbosa et al. 1996; Da Silva et al. 2000; Hernández-Monteagudo et al. 2000).

Combining the thermal Sunyaev-Zel'dovich effect and significant weak gravitational lensing therefore defines a large cluster sample. Figure 5 illustrates that a large portion of this sample is remarkably confined in redshift. Because of the exponential fall-off of the cluster population towards high mass, the sharp cut-off of the sample towards high redshift due to the Sunyaev-Zel'dovich selection criterion, and the fairly steep decline of lensing efficiency towards low redshifts, the majority of the combined Sunyaev-Zel'dovich-lensing cluster sample is confined to a narrow redshift interval around $z \approx 0.2$. This is further illustrated by the redshift distributions in Fig. 6.

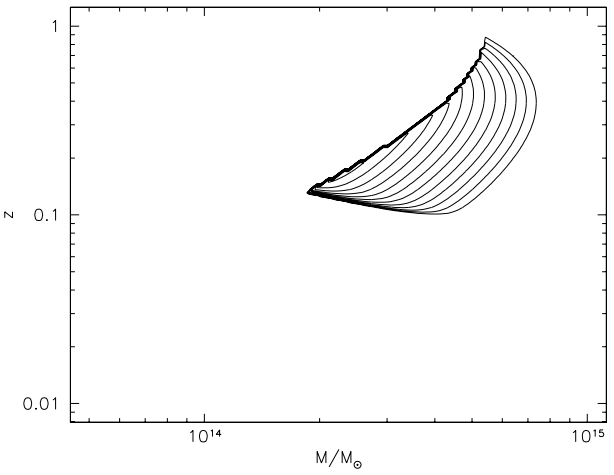

Fig. 5. Contours of the number density in the M-z plane of Sunyaev-Zel'dovich clusters detectable by *Planck* that are also efficient weak lenses. The contours range within (0.1−3.0) $10^{-10}\, M_\odot^{-1}$ in steps of 0.2 $10^{-10}\, M_\odot^{-1}$. A flat, low-density, cluster-normalised CDM model was assumed

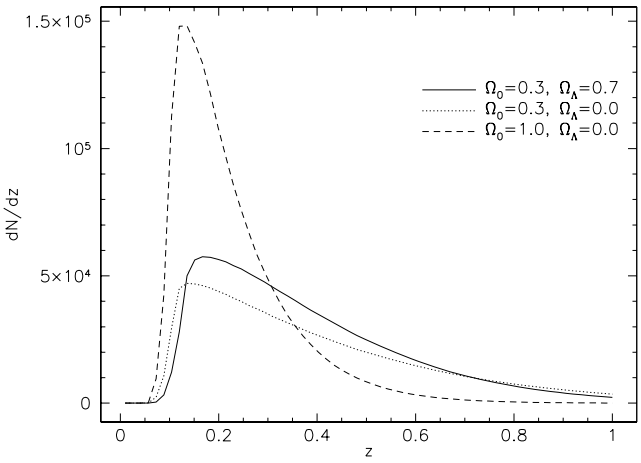

Fig. 6. Redshift distributions of lensing Sunyaev-Zel'dovich clusters for three different cosmological models, as indicated. The redshift distribution for $\Omega_0 = 1$ is cut off by rapid cluster evolution. For all cosmological models, the majority of clusters sits near $z = 0.1$−0.2

3.4. Analytic description of the sample

The main features of the region in M-z space occupied by lensing Sunyaev-Zel'dovich clusters can approximately be described analytically. Evidently, there are two sharp edges in the M-z plane which truncate the cluster population. The upper and lower edges, respectively, are due to the Sunyaev-Zel'dovich and lensing detection criteria. At low masses and redshifts, both edges are almost straight

lines in the double-logarithmically plotted Fig. 5, i.e. they are power laws. At $M \approx 5\ 10^{14}\,M_\odot$, the upper edge quite abruptly turns into the vertical. We will now explain these features.

Ignoring beam convolution and background effects, the upper edge approximately follows the line $z \propto M^{5/6}$: The integrated Compton-y parameter scales like $Y \propto TM/D_\mathrm{d}^2$, and the temperature $T \propto M^{2/3}$. For low redshifts, $D_\mathrm{d} \propto z$, hence $Y \propto M^{5/3}/z^2$. The relation $z \propto M^{5/6}$ then follows from the definition of the detection edge by $Y = Y_\mathrm{min} =$ constant. Figure 1 shows that the sample obtained with realistic detection criteria shows the same behaviour for cluster masses above $10^{14}\,M_\odot$.

An interesting deviation from this relation occurs at higher mass and redshift (see also Holder et al. 2000). The cluster temperature at a given mass increases with redshift like $(1+z)$, and the integrated Compton-y parameter diminishes with distance like D_d^{-2}. The angular-diameter distance D_d rises $\propto z$ for small redshifts and then flattens off. At a certain redshift, call it z_1, the ratio $D_\mathrm{d}^2(z)/(1+z)$ reaches a maximum, so that the integrated Compton-y parameter for a cluster of fixed mass first decreases with redshift out to z_1, and then increases again. For an Einstein-de Sitter universe, this happens for $z > z_1 = 7/9$, and for slightly higher z_1 in lower-density universes. Let M_1 be the lower mass limit for a cluster to be seen out to redshift z_1, then *all* clusters with masses $M \geq M_1$ will be detectable as Sunyaev-Zel'dovich sources, and they will also be significant lenses unless the background source distribution is narrow and located at low redshifts. Recent detections of efficienly lensing clusters at high redshifts (Luppino & Kaiser 1997; Clowe et al. 2000) show that this is unlikely to be the case. This explains the upturn of the upper edge of the contours in Fig. 5 near $M \approx 5\ 10^{14}\,M_\odot/h$. We should note, however, that the given explanation rests upon the assumption that clusters of fixed mass are hotter at higher redshifts, and that $T \propto (1+z)$. Should the true relation between temperature and redshift be flatter or steeper, the lower mass limit M_1 would increase or decrease, respectively. The sudden extension of the sample for $M \geq M_1$ therefore contains indirect information on the thermal history of the clusters. We will return to this point later.

On the other hand, the lower edge approximately follows $z \propto M^{-1/3}$: For low-redshift clusters, the ratio between the distances from the lens to the source and from the observer to the source is almost unity, hence the critical surface mass density is proportional to D_d^{-1} only. For low redshifts, $D_\mathrm{d} \propto z$, so that $\kappa_\mathrm{s} \propto z$. The lensing criterion $\mathcal{S} \geq \mathcal{S}_\mathrm{min}$ therefore implies $zr_\mathrm{s} \propto zM^{1/3} \geq$ const.

4. Mass distribution of the combined sample

4.1. Characteristic shape

Figure 7 shows that the mass distribution of lensing Sunyaev-Zel'dovich clusters has a characteristic shape, at least for low-density cosmologies.

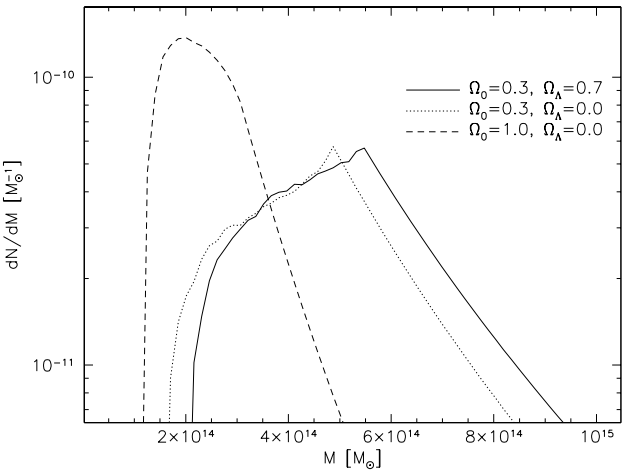

Fig. 7. Mass distribution of lensing Sunyaev-Zel'dovich clusters for three different cosmologies, as indicated. For low cosmic density, the curves have a characteristic shape: They rise abruptly near $2\ 10^{14}\,M_\odot$, flatten, reach a peak near $5\ 10^{14}\,M_\odot$, and then fall off exponentially. The mass distribution for high Ω_0 is shifted to lower masses and lacks the peak

The whole cluster sample is confined to the fairly narrow mass range. For low Ω_0, $2\ 10^{14} \leq M/M_\odot \leq 8\ 10^{14}$, and even narrower for high Ω_0. For low cosmic density, the mass distribution function abruptly rises at the low-mass end, flattens, peaks near $5\ 10^{14}\,M_\odot$, and then falls off exponentially. While the peak is pronounced for the low-density cosmologies, it is absent when Ω_0 is high.

Using the approximate analytic sample descriptions derived earlier for the number density of significantly lensing Sunyaev-Zel'dovich clusters in the M-z plane, the shape of the mass distribution is straightforwardly explained. All clusters can be seen above the mass M_1 introduced above. The high-mass end of the mass distribution therefore reflects the exponential cut-off expected from the Press-Schechter mass function (8). The peak in the mass distribution is given by M_1, i.e. the minimum mass for clusters to be visible out to the redshift z_1 where the squared angular-diameter distance, divided by $(1+z)$, reaches its maximum.

The cut-off at the low-mass end represents the lower-left corner of the contours in Fig. 5. It is defined by the intersection of two lines, $z = C_\mathrm{GL}\,M^{-1/3}$ from lensing, and $z = C_\mathrm{SZ}\,M^{5/6}$ from the Sunyaev-Zel'dovich effect, as explained before. We are dealing with low redshifts, so distances may be approximated by Hubble's law. For the low-density cosmological models, we can further neglect the redshift evolution of the cluster sample, i.e. we can set $D_+(z) = 1$ in (8). The number distribution of detectable clusters as a function of M can then be approximated by

$$\frac{\mathrm{d}N}{\mathrm{d}M} \propto \left(C_\mathrm{SZ}^3\,M^{5/6} - C_\mathrm{GL}^3\,M^{-8/3}\right) \times \exp\left[-\frac{1}{2}\left(\frac{M}{M_*}\right)^{2/3}\right], \qquad (34)$$

where we have inserted the Press-Schechter mass function (8) and put $n = -1$. This qualitatively explains the sudden rise in the mass distributions for the low-Ω_0 universes. For high Ω_0, cluster evolution is substantially faster. Therefore, there are essentially no clusters reaching the mass- and redshift limits (M_1, z_1) leading to the pronounced peak in the mass distributions. The low-mass cutoff, however, remains determined by the intersection of the Sunyaev-Zel'dovich and lensing sample edges.

4.2. Baryon fraction and Hubble constant

If observable, the distinct features in the mass distribution of lensing Sunyaev-Zel'dovich clusters have immediate physical implications. The first was already mentioned: All else fixed, the peak in the mass distribution contains indirect information on the thermal evolution of the cluster sample with redshift. Second, the exponential cut-off at the high-mass end allows to determine the cluster mass function at redshift $z \sim 0.2$, where the majority of the cluster sample is located. Third, the sharp cut-off at the low-mass end measures the intersection point between the two lines $z = C_{\rm GL}\, M^{-1/3}$ and $z = C_{\rm SZ}\, M^{5/6}$. For a fixed cosmological model, $C_{\rm GL}$ is fixed, while $C_{\rm SZ}$ is $\propto f_{\rm B} h$. Equating the two expressions leads to

$$M_0 \propto (f_{\rm B} h)^{-6/7}. \tag{35}$$

The higher the baryon fraction is, the lower is the mass limit for detectable Sunyaev-Zel'dovich clusters. Likewise, for higher Hubble constant, the angular-diameter distance to a fixed redshift is smaller, and lower-mass clusters can be seen. Third, the location of the peak, if it exists, is determined by the lowest mass required for a cluster to be seen beyond the maximum in $D^2(z)/(1+z)$. This is fixed by the Sunyaev-Zel'dovich detection criterion alone. It then follows from (10) that

$$M_1 \propto (f_{\rm B} h)^{-3/5}; \tag{36}$$

for increasing baryon fraction, the total cluster mass can be lower for the cluster to be seen, and likewise for a higher Hubble constant. Although in reality the relations between the low-mass cut-off and the peak position on the one hand and the baryon fraction on the other will be more complicated, these considerations show that the distinct features in the mass distribution contain information on various physical properties of the cluster population at moderate redshifts.

It appears from the foregoing discussion of the location of cut-off and peak in the mass function of the combined cluster sample, that baryon fraction and Hubble constant shift them in a completely parallel way. The real situation is somewhat more complex, for two reasons: First, Hubble constant and baryon fraction are further related through constraints from primordial nucleosynthesis. If $\Omega_{\rm B}$ is the density parameter of baryons, $f_{\rm B} = \Omega_{\rm B}/\Omega_0$, but primordial nucleosynthesis determines the physical baryon density, hence $\Omega_{\rm B}\, h^2$. Taking this into account, the baryon fraction itself scales with the Hubble constant as $f_{\rm B} \propto h^{-2}$. The diminution of the Sunyaev-Zel'dovich effect with decreasing Hubble constant as a consequence of increasing physical distances is therefore more than cancelled if the cluster baryon fraction follows the primordial nucleosynthesis constraint. Second, the Hubble constant also determines the shape parameter of the dark-matter power spectrum, $\Omega_0\, h$. Normalising the spectrum to the local abundance of rich clusters keeps the spectrum fixed at the linear cluster scale of $\approx 10\,{\rm Mpc}/h$. Lowering h shifts the peak of the spectrum to larger scales, leading to more power on larger and less power on smaller scales. This then leads to a higher abundance of more massive clusters. Figure 8 illustrates these effects.

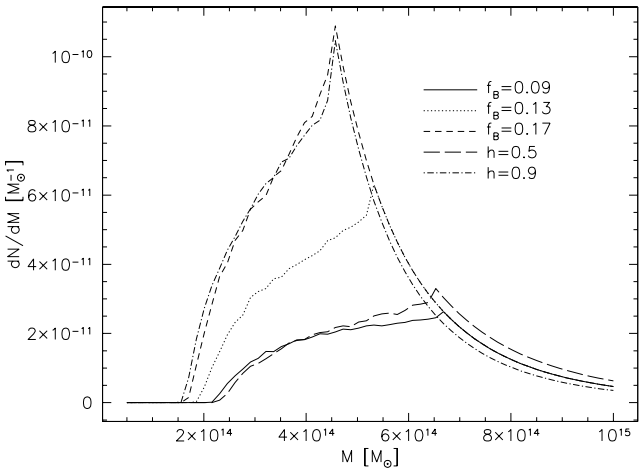

Fig. 8. Mass distributions in the combined Sunyaev-Zel'dovich and gravitational-lensing cluster sample, for different baryon fractions $f_{\rm B}$ and fixed Hubble constant, and for different Hubble constants and fixed baryon fraction, as indicated in the plot. The solid, dotted, and short-dashed curves show that an increasing baryon fraction shifts the peak to lower masses, as expected, and increases the peak height, while keeping the exponential cut-off constant. The dot-dashed, dotted, and long-dashed curves show that an increasing Hubble constant also shifts the peak towards lower masses, but also leads to lower amplitude in the exponential cut-off

The peak in the mass distribution shifts to lower masses as the baryon fraction or the Hubble constant increase. While the amplitude of the exponential cut-off is unchanged while h is kept fixed, it increases when h decreases, as expected. The most prominent effect is the change in the peak height with baryon fraction.

4.3. Mass determination

The simple relation between $M_{\rm ap}$ and the cluster mass M derived earlier and shown in Fig. 4 can now be used to derive cluster masses. Equations (27) and (30) imply

$$M_{\rm ap} = \left(\frac{3}{800\pi}\right)^{1/3} \frac{\delta_{\rm c}}{c}\, \frac{\rho_{\rm crit}^{2/3}}{\Sigma_{\rm cr}}\, M^{1/3} \equiv C_M\, M_{15}^{1/3}, \tag{37}$$

where $r_{\rm s} = r_{200}/c$ and the definition (1) of r_{200} have been inserted. Because of the fairly narrow redshift range

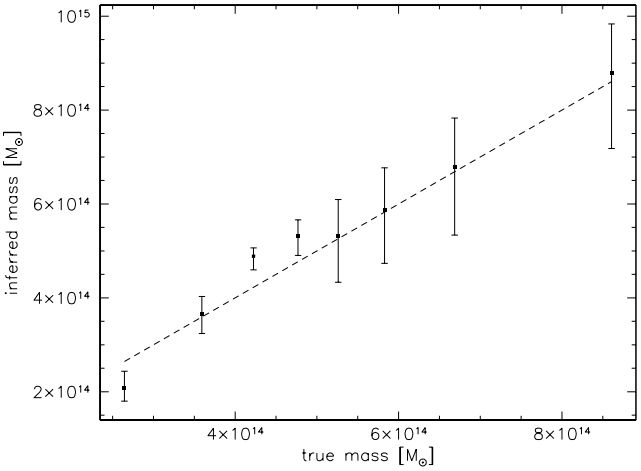

Fig. 9. Comparison of inferred and true masses of clusters drawn randomly from their expected mass-redshift distribution in a low-density, flat, cluster-normalised CDM model universe. The aperture mass $M_{\rm ap}(1')$ on an angular scale of $1'$ was calculated and converted to mass via Eq. (38). Each data point shows the median mass derived from an equal number of clusters. Error bars show the $\pm 34\%$ deviation from the mean, i.e. they would correspond to 1-σ error bars if the distribution was Gaussian

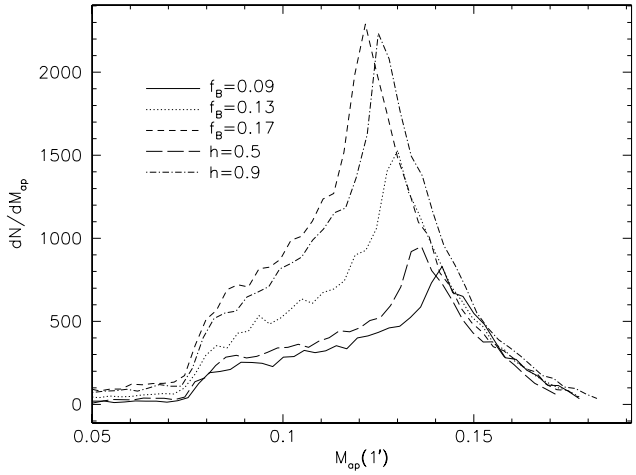

Fig. 10. Similar to Fig. 8, this figure shows the distribution of clusters as a function of $M_{\rm ap}$ rather than mass. Five curves are shown to illustrate the effects of changing baryon fraction and Hubble constant, as indicated

occupied by the cluster sample, and the low redshift where they are typically located, $\Sigma_{\rm cr}$ can be considered constant in redshift. What is more, C_M in (37) is almost independent of cosmological parameters. Changing Ω_0 from 0.3 to 1 changes C_M by less than 5 per cent. For an aperture radius of $1'$, we find

$$M_{\rm ap} \approx (0.18 \pm 0.01)\, M_{15}^{1/3}, \tag{38}$$

and this relation continues to hold even for moderatly high cluster redshifts. It is therefore straightforward to determine the absolute masses of the clusters in the combined gravitationally lensing Sunyaev-Zel'dovich cluster sample.

In order to test the accuracy of this mass determination, we have randomly drawn a set of clusters from the number-density distribution shown in Fig. 5, with the total number computed for a flat, low-density, cluster normalised CDM universe. For each of these clusters, we computed the aperture mass $M_{\rm ap}(1')$ for an aperture radius of $1'$, and then used Eq. (38) to infer its virial mass. Figure 9 compares the inferred and true masses, binned in such a way that each bin contains the same number of clusters.

Data points show the median of the inferred masses in each bin, and error bars enclose the $\pm 34\%$ deviation from the median, i.e. they loosely correspond to 1-σ error bars. As Fig. 9 shows, the accuracy of the inferred cluster masses is of order 20%. The distribution of clusters as a function of $M_{\rm ap}$ prominently reflects the peak in the mass distribution, as Fig. 10 shows.

Using (38), the true mass corresponding to the peak location in the mass function can accurately be determined from the peak in the $M_{\rm ap}$ distribution. The $M_{\rm ap}$ distribution shows the same behaviour in reaction to changes in baryon fraction and Hubble constant as the mass distribution shown in Fig. 8. In particular, the peak height changes substantially with the baryon fraction, and much less so with the Hubble constant.

Relation (38) holds for clusters with an NFW density profile. It is valid because the aperture-mass profile is essentially flat for small aperture sizes, so that a weak-lensing estimate inside an area with fixed angular size can be used to extract a global halo property. Generally, the cluster mass profile needs to be known in order to relate aperture masses to virial masses. Surface-density profiles of clusters can be constrained with the same weak-lensing data used to determine the aperture masses, so that masses can be determined from weak lensing even if the true profile deviates from the NFW form.

However, the conversion from aperture mass to virial mass is not necessary for the extraction of cosmological information from the combined gravitationally lensing Sunyaev-Zel'dovich cluster sample. Rather, one can use weak-lensing quantities to classify clusters, and then use direct weak-lensing simulations to compare models to data.

5. Summary

Full-sky microwave surveys like the upcoming *Planck* mission will detect of order 10^4 galaxy clusters through their thermal Sunyaev-Zel'dovich effect. Using modified Press-Schechter theory in CDM model universes normalised to the local abundance of rich clusters, and scaling relations derived from the spherical collapse model, we have investigated the physical properties which that cluster sample is expected to have. We have then addressed the question what additional information can be gained by weak-lensing follow-up observations of the clusters in the Sunyaev-Zel'dovich sample. For doing so, we described individual clusters with the density profile of

Navarro et al. (1997) and applied the aperture mass as a measure for their weak-lensing effects. Our main results can be summarised as follows:

- Taking beam convolution and background fluctuations into account, the number of Sunyaev-Zel'dovich clusters detectable for *Planck* is a few times 10^4 if a baryon fraction of 13% is kept fixed, quite independent of the cosmological parameters. If the baryon fraction is adapted to the primordial nucleosynthesis constraint, it drops with increasing Ω_0, and the number of detectable Sunyaev-Zel'dovich clusters falls by a factor of $\sim$3 as Ω_0 increases from 0.3 to 1;
- One particular measure of weak gravitational lensing, the aperture mass, effectively determines the convergence scale κ_s for a cluster described by an NFW density profile, and the Einstein radius for a singular isothermal sphere. The aperture-mass profile of clusters depends sensitively on the density profile. While it falls with aperture size θ as θ^{-1} for singular isothermal spheres, it is much flatter for a NFW haloes;
- The significantly lensing sub-sample comprises more than 70% of the original Sunyaev-Zel'dovich cluster sample. The combined sample is narrowly confined in redshift and mass. The majority of redshifts fall within 0.2 ± 0.1, and the masses within $(5 \pm 3)\ 10^{14}\,M_\odot$. Approximate analytic descriptions of the sample's number density in the M-z plane are given;
- Because of the narrow redshift range and the generally low cluster redshifts, the weak-lensing effects are virtually independent of the source redshift distribution. Under these circumstances, the aperture mass essentially measures the radial scale of the NFW density profile, which can easily be converted to virial mass. The relation $M_\mathrm{ap} \propto M^{1/3}$ holds to very good approximation. Cluster masses can be determined with that relation with an accuracy of $\sim$20%;
- The mass distribution of the combined cluster sample exhibits a sharp low-mass cutoff and an exponential decrease at high masses. For low-density universes, the mass distribution has a sharp peak near $5\ 10^{14}\,M_\odot$. The low-mass cutoff is due to the lack of significant lensing effects in low-mass Sunyaev-Zel'dovich clusters, since they have low redshifts. The high-mass fall-off reflects the exponential decline in the cluster mass function. The peak occurs at the minimum mass required for a cluster to be a detectable Sunyaev-Zel'dovich source at all redshifts. This is possible because the squared angular diameter distance, divided by $(1+z)$, has a maximum at a finite redshift $z_1 \lesssim 1$. The peak occurs if clusters exist at such redshifts, i.e. in low-density universes;
- The cluster mass at the peak location can accurately be measured if the cluster density profile is known. In combination with the exponential high-mass cut-off of the mass distribution, the peak location allows the determination of the amplitude of the dark-matter power spectrum and the baryon fraction in the intracluster gas.

Of course, we rely on the validity of Press-Schechter theory, as modified by Sheth & Tormen (1999) and Jenkins et al. (2001). The mass function derived by Jenkins et al. from numerical simulations agrees very well with the analytical expression by Sheth & Tormen, showing that there are good reasons to believe that the mass function used here approximates reality sufficiently closely.

Although all our results were derived under the assumption that clusters have the density profile found by Navarro et al. (1997), this assumption is not critical for the results. The property shown, that the aperture mass becomes independent of aperture size for small apertures, is convenient for our purpose in that it facilitates the conversion of aperture masses to virial masses, but by no means necessary. The NFW density profile has recently been disputed by studies finding a steeper central density cusp (e.g. Moore et al. 1999), albeit on radial scales much smaller than probed by weak-lensing techniques. Weak lensing observations will allow the determination of the mass profile. The fact that the combined gravitationally lensing Sunyaev-Zel'dovich cluster sample is confined to a fairly narrow, low-redshift range implies that weak-lensing results become essentially independent of the source-redshift distribution.

It therefore appears safe to conclude that cluster samples selected by their thermal Sunyaev-Zel'dovich effect and combined with weak-lensing follow-up observations, are well confined in redshift and mass, and provide a unique opportunity to accurately measure the cluster mass function at redshifts around 0.2, thus the amplitude of the dark-matter power spectrum, and the baryon fraction in the intracluster gas.

The most prominent feature in the mass function of the combined gravitationally lensing, Sunyaev-Zel'dovich cluster sample is the pronounced peak predicted to occur for low-density universes. Its physical origin is the flattening of the relation between angular-diameter distance and redshift away from Hubble's law due to space-time curvature, and the thermal history of the cluster population, for which the spherical collapse model predicts that temperature rises as $(1+z)$ for fixed cluster mass. Adopting this model, we saw that location and height of the peak provide additional information on the intracluster baryon fraction. It is highly likely that the microwave background observations leading to the compilation of the Sunyaev-Zel'dovich cluster sample will allow accurate determinations of the cosmological parameters including the baryon fraction (e.g. Efstathiou & Bond 1999). The gravitational-lensing follow-up observations will then supply valuable tests for the consistency between the detected and expected cluster populations, and additional information on the thermal history of the cluster population.

Finally, it appears recommendable to avoid the conversion from weak-lensing measures like the aperture mass to virial mass. It is equally possible to define a cluster

sample not by its mass, but operationally by the integrated Sunyaev-Zel'dovich decrement or increment and weak-lensing measures like the aperture mass. Comparing Figs. 8 and 10 shows that the aperture-mass distribution exhibits the same features as the mass distribution itself. Uncertainties in the conversion between lensing effects and masses could be avoided if measured aperture-mass distributions would directly be compared to simulations such as those leading to the results shown in Fig. 10.

Acknowledgements. I wish to thank Lauro Moscardini, Adi Nusser, Peter Schneider and Saleem Zaroubi for enlightening discussions, and Simon White for detailed comments on the manuscript.

References

Aghanim, N., De Luca, A., Bouchet, F. R., Gispert, & Puget, R. J.-L. 1997, A&A, 325, 9
Barbosa, D., Bartlett, J. G., Blanchard, A., & Oukbir, J. 1996, A&A, 314, 13
Bartelmann, M. 1996, A&A, 313, 697
Bartelmann, M., & Schneider, P. 2001, PhR, 340, 291
Bartlett, J. G. 2000, preprint [astro-ph/0001267], submitted to A&A
Bersanelli, M., et al. 1996, Report on Phase A Study for COBRAS/SAMBA, European Space Agency, Paris
Birkinshaw, M. 1999, PhR, 310, 97
Bower, R. G. 1997, MNRAS, 288, 355
Clowe, D., Luppino, G. A., Kaiser, N., & Gioia, I. M. 2000, ApJ, 539, 540
Da Silva, A. C., Barbosa, D., Liddle, A. R., & Thomas, P. A. 2000, MNRAS, 317, 37
Eftstathiou, G., & Bond, J. R. 1999, MNRAS, 304, 75
Eke, V. R., Cole, S., & Frenk, C. S. 1996, MNRAS, 282, 263
Eke, V. R., Navarro, J. F., & Frenk, C. S. 1998, ApJ, 503, 569
Evrard, A. E., & Henry, J. P. 1991, ApJ, 383, 95
Grego, L., Carlstrom, J. E., Marshall, K. J., et al. 2000, ApJ, 539, 39
Haehnelt, M. G. 1997, in Microwave Background Anisotropies, ed. F. R. Bouchet, R. Gispert, B. Guiderdoni, & J. Tran Thanh Van (Gif-sur-Yvette: Éditions Frontières)
Hernández-Monteagudo, C., Atrio-Barandela, F., & Mücket, J. P. 2000, ApJ, 528, L69
Hobson, M. P., Jones, A. W., Lasenby, A. N., & Bouchet, F. R. 1998, MNRAS, 300, 1
Holder, G. P., Mohr, J. J., Carlstrom, J. E., Evrard, A. E., & Leitch, E. M. 2000, ApJ, 544, 629
Jenkins, A., Frenk, C. S., White, S. D. M., et al. 2001, MNRAS, 321, 372
Kaiser, N. 1986, MNRAS, 222, 323
Kaiser, N. 1991, ApJ, 383, 104
Kruse, G., & Schneider, P. 1999, MNRAS, 302, 821
Luppino, G. A., & Kaiser, N. 1997, ApJ, 475, 20
Mathiesen, B. F., & Evrard, A. E. 2001, ApJ, 546, 100
Mohr, J. J., Mathiesen, B. F., & Evrard, A. E. 1999, ApJ, 517, 627
Moore, B., Quinn, T., Governato, F., Stadel, J., & Lake, G. 1999, MNRAS, 310, 1147
Myers, S. T., Baker, J. E., Readhead, A. C. S., & Leitch, E. M. 1997, ApJ, 485, 1
Navarro, J. F., Frenk, C. S., & White, S. D. M. 1995, MNRAS, 275, 720
Navarro, J. F., Frenk, C. S., & White, S. D. M. 1997, ApJ, 490, 493
Press, W. H., & Schechter, P. 1974, ApJ, 187, 425
Puget, J.-L., et al. 1998, High Frequency Instrument for the *Planck* Mission, proposal in response to ESA's Announcement of Opportunity
Rephaeli, Y. 1995, ARA&A, 33, 541
Richstone, D. O., Loeb, A., & Turner, E. L. 1992, ApJ, 393, 477
Schneider, P. 1996, MNRAS, 283, 837
Schramm, D. N. 1998, in Eighteenth Texas Symposium on Relativistic Astrophysics and Cosmology, ed. A. V. Olinto, J. A. Frieman, & D. N. Schramm (Singapore: World Scientific)
Sheth, R. K., & Tormen, G. 1999, MNRAS, 308, 119
Sheth, R. K., Mo, H. J., & Tormen, G. 1999, MNRAS, submitted, preprint [astro-ph/9907024]
Smail, I., Hogg, D. W., Yan, L., & Cohen, J. G. 1995, ApJ, 449, L105
Stoehr, F. 1999, High Resolution Simulations of Underdense Regions, Diploma Thesis, Munich: Technical University
Sunyaev, R. A., & Zel'dovich, Y. B. 1972, Comm. Astrophys. Space Phys., 4, 173
Sunyaev, R. A., & Zel'dovich, Y. B. 1980, ARA&A, 18, 537
Viana, P. T. P., & Liddle, A. R. 1999, MNRAS, 303, 535
White, S. D. M., Efstathiou, G., & Frenk, C. S. 1993, MNRAS, 262, 1023